WILEY InterScience® DISCOVER SOMETHING GREAT

PROTEINS STRUCTURE ■ FUNCTION ■ BIOINFORMATICS

Kinetically driven refolding of the hyperstable EBNA1 origin DNA-binding dimeric β-barrel domain into amyloid-like spherical oligomers

Eleonora Freire[1], Cristian Oddo[1], Lori Frappier[2], and Gonzalo de Prat-Gay[1]*

[1] Instituto Leloir, Patricias Argentinas 435, (1405) Buenos Aires, Argentina

[2] Department of Medical Genetics and Microbiology, University of Toronto, Toronto, Ontario, Canada M5S 1A8

ABSTRACT

The Epstein-Barr nuclear antigen 1 (EBNA1) is essential for DNA replication and episome segregation of the viral genome, and participates in other gene regulatory processes of the Epstein-Barr virus in benign and malignant diseases related to this virus. Despite the participation of other regions of the protein in evading immune response, its DNA binding, dimeric β-barrel domain (residues 452–641) is necessary and sufficient for the main functions. This domain has an unusual topology only shared by another viral origin binding protein (OBP), the E2 DNA binding domain of papillomaviruses. Both the amino acid and DNA target sequences are completely different for these two proteins, indicating a link between fold conservation and function. In this work we investigated the folding and stability of the DNA binding domain of EBNA1 OBP and found it is extremely resistant to chemical, temperature, and pH denaturation. The thiocyanate salt of guanidine is required for obtaining a complete transition to a monomeric unfolded state. The unfolding reaction is extremely slow and shows a marked uncoupling between tertiary and secondary structure, indicating the presence of intermediate species. The Gdm.SCN unfolded protein refolds to fully soluble and spherical oligomeric species of 1.2 MDa molecular weight, with identical fluorescence centre of spectral mass but different intensity and different secondary structure. The refolded spherical oligomers are substantially less stable than the native recombinant dimer. In keeping with the substantial structural rearrangement in the oligomers, the spherical oligomers do not bind DNA, indicating that the DNA binding site is either disrupted or participates in the oligomerization interface. The puzzling extreme stability of a dimeric DNA binding domain from a protein from a human infecting virus in addition to a remarkable kinetically driven folding where all molecules do not return to the most stable original species suggests a co-translational and directional folding of EBNA1 in vivo, possibly assisted by folding accessory proteins. Finally, the oligomers bind Congo red and thioflavin-T, both characteristic of repetitive β-sheet elements of structure found in amyloids and their soluble precursors. The stable nature of the "kinetically trapped" oligomers suggest their value as models for understanding amyloid intermediates, their toxic nature, and the progress to amyloid fibers in misfolding diseases. The possible role of the EBNA1 spherical oligomers in the virus biology is discussed.

Proteins 2008; 70:450–461.

Key words: Epstein-Barr; EBNA1; DNA binding; folding; oligomers; amyloid; β-barrel.

INTRODUCTION

Double-stranded DNA replication starts with the binding of an initiator protein to a specific nucleotide sequence, termed the origin. Proteins that bind to replication origins of cells, virus, and plasmids are known as origin binding proteins (OBPs). OBPs facilitate local distortion or unwinding of the origin DNA and nucleate the assembly of the DNA replication apparatus through specific interactions with other replication proteins. One of the OBPs, Epstein-Barr virus nuclear antigen 1 (EBNA1) from the Epstein-Barr virus (EBV), binds specifically to origin sequences and relies on other factors to accomplish the unwinding. EBV is an ubiquitous human gamma herpes virus that is associated with several diseases and malignancies. The crystal structure of EBNA1 free or bound to DNA revealed a particular fold, an eight stranded dimeric β-barrel where each monomer contrib-

The Supplementary Material referred to in this article can be found online at http://www.interscience.wiley.com/jpages/0887-3585/suppmat.
Grant sponsor: Wellcome Trust; Grant number: 066649/Z/01/Z; Grant sponsor: ANPCyT; Grant number: PICT2004 15-26043; Grant sponsor: Canadian Institutes of Health Research (CIHR).
*Correspondence to: Gonzalo de Prat-Gay, Instituto Leloir, Patricias Argentinas 435, (1405) Buenos Aires, Argentina. E-mail: gpratgay@leloir.org.ar
Received 5 September 2006; Revised 19 December 2006; Accepted 19 February 2007
Published online 6 August 2007 in Wiley InterScience (www.interscience.wiley.com). DOI: 10.1002/prot.21580

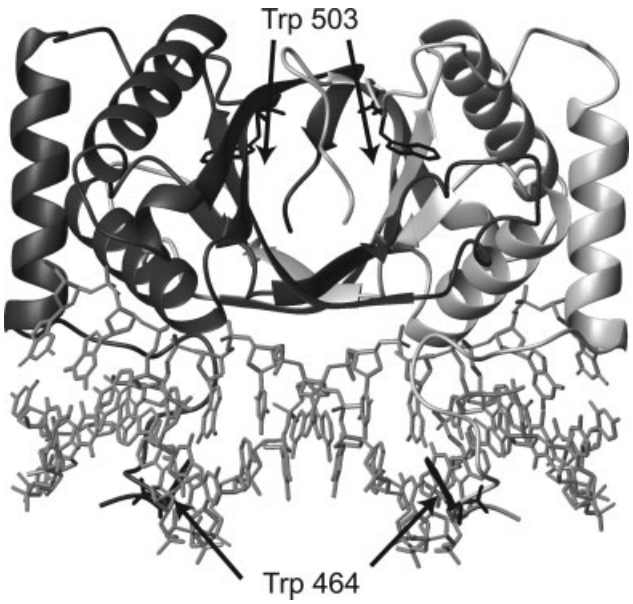

Figure 1

The dimeric β-barrel fold. Structure of EBNA1$_{459–607}$ DNA binding domain bound to DNA. Front view (Swiss PDB viewer software). Trp 464 and Trp 503 are shown in the figure.

utes with four antiparallel β-strand (Refs. 1 and 2, Fig. 1). This fold is remarkably similar to that of the papillomavirus E2 DNA binding domain, another viral OBP and transcriptional regulator.[3] This structural homology was unexpected as the proteins share no sequence homology and the Epstein-Barr and papillomaviruses are not evolutionary related. We have been investigating the folding mechanism of the human papillomavirus type 16 (HPV16) E2 DNA binding domain[4–8] and we now address the folding mechanism of EBNA1 in an attempt to understand topological conservation in distant viral proteins.

EBNA1 is the only EBV protein required for the replication and stable maintenance of EBV genomes in latently infected cells. EBNA1 is known to play three important roles that require specific binding to EBV DNA sequences in the latent origin of replication (oriP): the initiation of DNA replication, viral DNA segregation, and transcriptional activation. A protease-resistant domain in the C-terminus of EBNA1 (amino acids 452–641) is required and sufficient for DNA recognition and dimerization of EBNA1.[9,10] Analyses of the DNA binding properties of EBNA1, EBNA1$_{452–641}$, show it to be virtually identical to full length EBNA1 in terms of DNA binding affinity, specificity, and cooperativity.[11,12]

The fact that EBNA1 and E2 share similar topology and are OBPs suggests a link between the unusual folding topology and the function. Studies of the folding mechanism of monomeric proteins have been the major focus in efforts to describe the protein folding.[13,14] Significant insights have been gained from monomeric folding systems regarding the intramolecular forces responsible for the productive formation and stabilization of secondary and tertiary structures. In contrast, the folding of oligomeric proteins is often more complex and requires the formation of secondary and tertiary structure as well as productive quaternary interactions necessary for biological function. Folding experiments on large, oligomeric proteins demonstrated the complexity of this coordination of multiple levels of structure formation.[15–17] Good smaller oligomeric folding models of coupling of secondary, tertiary, and quaternary structure are dimeric proteins, for example, the P22 Arc repressor[18,19] and the GCN-4-derived leucine zipper peptides.[20,21] Some dimers have the particularity that the folding of each monomer depends on the formation of the interface of the dimer. However, just as with monomeric systems, larger dimers tend to follow more complex folding mechanism, with transient kinetic intermediates and sometimes parallel pathways. Examples include the C-terminal domain of papillomavirus E2,[22] ketosteroid isomerases,[23,24] *Escherichia coli* Trp repressor,[25–27] glutathione transferases,[28,29] and bacterial luciferase.[30–32]

In the present work, we investigate the folding properties of the DNA binding domain of EBNA1 (EBNA1$_{452–641}$). We found it is extremely resistant to chemical denaturants, temperature, and pH. The domain can be only unfolded completely using guanidinium thiocyanate (Gdm.SCN). The folding is reversible but the refolded species is a spherical-shaped oligomer of 45 nm diameter, as judged by atomic force microscopy (AFM). Circular dichroism (CD), fluorescence spectroscopy, and light scattering were used to characterize the oligomeric structure. This oligomer is much less stable than the dimer and cannot bind DNA, which strongly suggests a substantially different topology, product of a kinetically driven reaction.

EXPERIMENTAL PROCEDURES

Purification of recombinant EBNA1$_{452–641}$

The EBNA1$_{452–641}$ domain was expressed in *Escherichia coli* BL21(DE3). Bacterial cells expressing EBNA1$_{452–641}$ were grown in a Bio Flo110 Modular Benchtop Fermentor (1.5 L) in Terrific broth at 37°C to an absorbance of 0.5 at 600 nm, and EBNA1$_{452–641}$ expression was induced with 0.5 m*M* isopropyl β-D-thiogalactopyranoside, followed 3 h later by the addition of 150 μg/mL of rifampicin. After overnight postinduction the cells were harvested by centrifugation and suspended in 0.1 vol of the lysis buffer (100 m*M* Tris HCl pH 6.8, 600 m*M* NaCl, 1.0 m*M* EDTA, 1.0 m*M* phenylmethylsulfonyl fluoride, and 10 m*M* 2-mercaptoethanol). Cells were frozen at −70°C and then thawed and lysed by sonication at 0°C twice. The lysate was clarified by centrifugation at 20,000*g* for 20 min. The supernatant was then placed in

a 75°C water bath until the temperature of the protein solution reached the temperature of the bath. Heating was followed by a 10-min incubation on ice. The supernatant was clarified by centrifugation at 20,000*g* for 40 min and then loaded onto Heparin HyperD (BioSepra, Villeneuve la Garenne, France) affinity column equilibrated with buffer A (50 m*M* Tris-HCl (pH 7.2), 0.2*M* NaCl, and 5 m*M* 2-mercaptoethanol), and washed with 5 column volumes of the same buffer and eluted with 0.15–1.0*M* NaCl linear gradient. The fractions that were over 90% pure were pooled, dialyzed against buffer A without 2-mercaptoethanol, and digested with thrombin (1.5 units/mg of protein) at 37°C for 7 h in order to remove the 6xHis-tag. After digestion was stopped with 0.2 m*M* phenylmethylsulfonyl fluoride, the protein was loaded onto a Mono Q ion exchange column (Pharmacia Biotech, Uppsala, Sweden) equilibrated with buffer A and washed with 5 column vol of the same buffer. The column was subjected to a 15 mL linear gradient from 0.2 to 1.0*M* NaCl in buffer A. The fractions that were greater than 95% pure (as judged by Coomassie staining of 15% SDS-polyacrylamide gels) were pooled, concentrated using Centriprep-10 (Amicon, Bedford, MA), and loaded onto a Superdex 75 gel filtration column. This procedure yielded around 20 mg/mL of over 98% pure $EBNA1_{452–641}$. The purified protein was dialyzed against 25 m*M* Tris HCl pH 7.2, 500 m*M* NaCl, 0.2 m*M* EDTA, 10% glycerol, and 5 m*M* 2-mercaptoethanol, and stored as a 150 μ*M* solution at −70°C after snap freezing in liquid nitrogen. Protein concentration was determined using an extinction coefficient of $4.19 \times 10^4 M^{-1}\ cm^{-1}$.

Size exclusion chromatography

Gel filtration experiments were performed in a Superdex 75 (3×10^3 to 7×10^4 Da range, Pharmacia Biotech) and in a Sephacryl S-500 (2×10^4 to 8×10^6 Da range, Pharmacia Biotech) column at 1 mL/min, previously equilibrated in the same buffer Tris 25 m*M* pH 7.5 and 0.2*M* NaCl. Absorbance at 280 nm was recorded. $EBNA1_{452–641}$ samples were centrifuged 15 min at 10,000*g* before injection. For Gdm.SCN experiments, both protein samples (30 μ*M*) and the column were equilibrated at the indicated denaturant concentrations before injection (figure in supplementary material).

Spectroscopy

CD measurements were carried out in a Jasco J-810 instrument (Jasco, Japan), far-UV spectra were collected using a Peltier temperature-controlled sample holder in a 0.1 cm path length cell, with a protein concentration range of 4–20 μ*M*. Fluorescence emission spectra were recorded on an Aminco Bowman spectrofluorimeter with an excitation wavelength of 290 nm and measuring the emission wavelength at 335 nm. Thioflavin T emission spectra were recorded at excitation and emission wavelengths of 435 and 480 nm, respectively, at a protein concentration of 2 μ*M* in 25 m*M* sodium phosphate buffer pH 8 and 5 μ*M* thioflavin T. For Congo red binding experiments, a 400–600 nm spectrum of the buffer (10 m*M* Tris-HCl pH 8, 0.2*M* NaCl, and 1 m*M* DTT) plus the protein solution (10 μ*M*) was subtracted from a spectrum of the buffer (10 m*M* Tris-HCl pH 8, 0.2*M* NaCl, and 1 m*M* DTT) plus the protein solution (10 μ*M*) plus Congo red (5 μ*M*). This spectrum was compared with the spectrum of buffer plus Congo red (5 μ*M*), which have been background-corrected by subtracting a spectrum containing only buffer (10 m*M* Tris-HCl pH 8, 0.2*M* NaCl, and 1 m*M* DTT). A red shift of the maximum Congo red absorbance from 480 nm to 500–510 nm and an intensity increase were taken as indicative of positive reaction. The absorbance spectrum was measured with a Jasco V-550 spectrophotometer at 25°C.

Fluorescence measurements for DNA binding studies were recorded in a Aminco Bowman series 2 luminescence spectrometer assembled in "L" geometry. For fluorescein anisotropy measurements, excitation was set to 490 nm with 4 nm band path and emission was recorded at 518 nm. The temperature was kept constant at (25 ± 0.1)°C through all experiments. For monitoring transitions we use the center of spectral mass (CSM), where we accumulate 10 scans and then calculate the wavenumber in cm^{-1} at which the area of the spectra is divided in two identical areas. The spectrum of aminoacid tryptophan molecule in solution yields three fluorescent bands; if we add the changing environment in a protein and add different residues in different environments, calculating the maximum wavelength from a wide complex spectra is not accurate enough.[33] Fluorescence intensity is subjected to bleaching and to electronic fluctuations. Errors in CSM measurements are less than 5%.

Titrations were performed adding small amounts of a concentrated solution of the protein to fixed amounts of a concentrated solution of the DNA and allowed to equilibrate for 2 min. In all cases, maximal dilution was 20%, and the data were corrected accordingly.

Light scattering

The weight average molecular weight (Mw) of $EBNA1_{452–641}$-SOs was determined on a Precision Detectors PD2010 light scattering instrument tandemly connected to a high-performance liquid chromatography system coupled to a LKB 2142 differential refractometer. In general, 500 μL of $EBNA1_{452–641}$-SOs (0.5 mg/mL) or 95–200 μL of $EBNA1_{452–641}$ (0.5–4.2 mg/mL) was loaded on a Sephacryl S-500 (Pharmacia Biotech) or a Superdex 75 (Pharmacia Biotech) column and eluted with 25 m*M* Tris or 20 m*M* citrate/phosphate buffer, under different pH, Gdm.SCN, and NaCl conditions. The 90° light scattering and refractive index signals of the eluting material

DOI 10.1002/prot

were recorded on a PC computer and analyzed with the Discovery32 software supplied by Precision Detectors. The 90° light scattering detector was calibrated using bovine serum albumin (Mw: 66.5 kDa) as a standard.

Atomic force microscopy

For AFM imaging, protein $EBNA1_{452-641}$ and $EBNA1_{452-641}$-SOs were diluted to 2 ng/μL in buffer containing 10 m*M* HEPES, pH 7.5, and 1 m*M* $MgCl_2$. 20 μL of the mixture were deposited onto freshly cleaved muscovite mica. After 2–5 min, the sample was gently washed with 0.5 mL milli-Q water to remove molecules that were not firmly attached to the mica and blown dry with nitrogen. Tapping-mode AFM was performed using a Nanoscope III Multimode-AFM (Digital Instruments, Veeco Metrology, Santa Barbara, CA) with a J-type piezoelectric scanner with a maximal lateral range of 120 μm. Micro-fabricated silicon cantilevers of 125 μm in length and a force constant of 40 N/m were used (NanoDevices, Veeco Metrology, Santa Barbara, CA). Cantilever oscillation frequency was tuned to the resonance frequency of the cantilever (280–350 kHz). After a period of 15–30 min of thermal relaxation, initial engagement of the tip was achieved at scan size zero to minimize sample deformation and tip contamination. The images (512 × 512 pixels) were captured with a scan size of between 0.5 and 3 μm at a scan rate of 1–2 scan lines/s. Images were processed by flattering using Nanoscope software (Digital Instruments) to remove background slope. For the statistical analysis, the diameter was measured in the middle of the height of the cross-section.

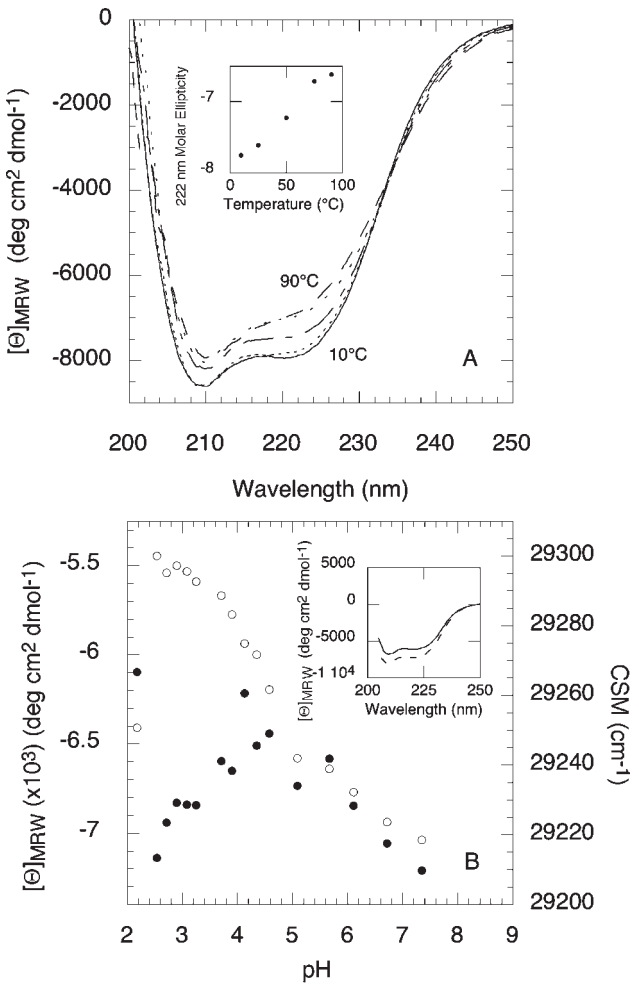

Figure 2

*pH and thermal stability of the $EBNA1_{452-641}$ dimer. (**a**) Temperature-dependent conformational changes monitored by CD from T = 10°C to T = 90°C. [$EBNA1_{452-641}$] = 6.5 μM. Buffer: Phosphate 10 mM pH 7. Inset: temperature-dependent changes monitored by CD at 222 nm. (**b**) Fluorescence and CD changes in the pH transitions of $EBNA1_{452-641}$. CSM was calculated from fluorescence emission between 300 and 450 nm. Inset: pH dependent conformational changes monitored by CD from pH 2.2 (continuous line) through 7.4 (dashed line). [$EBNA1_{452-641}$] = 4 μM. Buffer: citrate/phosphate 25 mM and NaCl 0.2M.*

RESULTS

Extreme resistance of $EBNA1_{452-641}$ to pH, temperature, and chemical denaturation

The far-UV CD spectrum of the $EBNA1_{452-641}$ domain has the characteristic bands for α-helix, namely at 208 and 222 nm [Fig. 2(a)], despite containing a significant amount of β-sheet structure. The fluorescence spectrum is consistent with tryptophan residues being buried from the solvent, with a maximum at ∼330 nm (see below). Analysis of the pH transition shows small changes in secondary and tertiary structure: 7% of the total change in CSM upon global unfolding of the tryptophan and 17% of the ellipticity change [Fig. 2(b)]. The far-UV CD and fluorescence changes take place in parallel up to pH 4.2 where a biphasic behavior is observed for the ellipticity. However, no indication of global unfolding is observed since only at pH 2.2, the protein starts to loose its native tertiary structure only partially: after 16 h at that pH, the far-UV CD spectrum corresponds to a protein in a folded conformation [Fig. 2(b), inset]. Light scattering experiments at pH 3.6 and 7.0 (Table I) yield an identical molecular weight (44 kDa) and radius (3.5 nm), indicating that at low pH, the protein remains as a rather compact dimer.

The CD spectra at increasing temperatures present small but significant changes, and a folded structure is evident even at 90°C [Fig. 2(a)]. A conformational transition corresponding to 28% of the change expected for global unfolding takes place; however, with an apparent t_m of ∼55°C [Fig. 2(a), inset]. This transition likely involves a local rearrangement rather than global unfolding by a small population of molecules.

To analyze the stability of $EBNA1_{452-641}$ to unfolding, we carried out chemical denaturation experiments using

Table I
Molecular Weight and Size Determination of EBNA1$_{452–641}$ Species by Light Scattering

	Molecular weight (Da)	Radius (nm)
pH 7.0	43,680	3.6
pH 3.6	44,180	3.5
pH 7.0, 4*M* Gdm.SCN	19,200	n.d.
pH 7.0 Refolded[a]	1,230,000	19

[a]EBNA1$_{452–641}$-SOs.

guanidinium chloride (Gdm.Cl) at pH 3.0, 7.0, and 10.0, following the changes in the CSM of the fluorescence spectrum [Fig. 3(a)]. As a comparison, we carried out a Gdm.Cl unfolding experiment for the DNA binding domain of HPV16 E2 at pH 7.0 in identical conditions to EBNA1$_{452–641}$. Unlike EBNA1$_{452–641}$, the E2 DNA binding domain displays a complete unfolding transition with a [Gdm.Cl]$_{50\%}$ of 2.7*M*, compared to 6.3*M* for the EBNA1$_{452–641}$ domain [Fig. 3(a)].

In an attempt to observe a phase indicative of a dissociation of the dimer, we carried out the same experiment and monitored anisotropy of the tryptophan residue. The transition takes place in absolute parallel with the main transition followed by CSM [Fig. 3(b)]. In addition, we carried out gel filtration experiments of EBNA1$_{452–641}$ preincubated at different representative Gdm.SCN concentrations each chromatographed in the indicated denaturant concentration. There is no evidence of a monomer being formed at any condition, and there is only one peak in all conditions, indicating a fast exchange between folded and unfolded species (see supplementary materials). The elution volumes, taking folded dimer and unfolded monomer as extremes, were plotted [Fig. 3(b)] and considering the low resolution of the technique change concomitantly with CSM and anisotropy. Unfortunately, Gdm.SCN precludes the use of far-UV circular dichroism.

The dimeric domain displays an unusually high stability towards Gdm.Cl, and the solubility of the salt limits the possibility of obtaining a clear baseline for the unfolded state. This high stability is evident even at the extreme pHs 3.0 and 10.0. We switched to a stronger denaturant, guanidinium thiocyanate (Gdm.SCN), so that a complete transition could be obtained, and a clear unfolded state baseline is observed [Fig. 3(b)]. A 2-h incubation appears to be enough to complete the global unfolding process, but a small shift in the 24-h experiment might suggest some degree of a slower unfolding phase (not shown). Surprisingly, there is no concentration dependence of the unfolding transition in the concentration range of 0.1–5 μ*M* (not shown). Although Gdm.SCN allows the observation of the full transition, it introduces too much noise for the determination of the change of the ellipticity upon unfolding. In any case, at

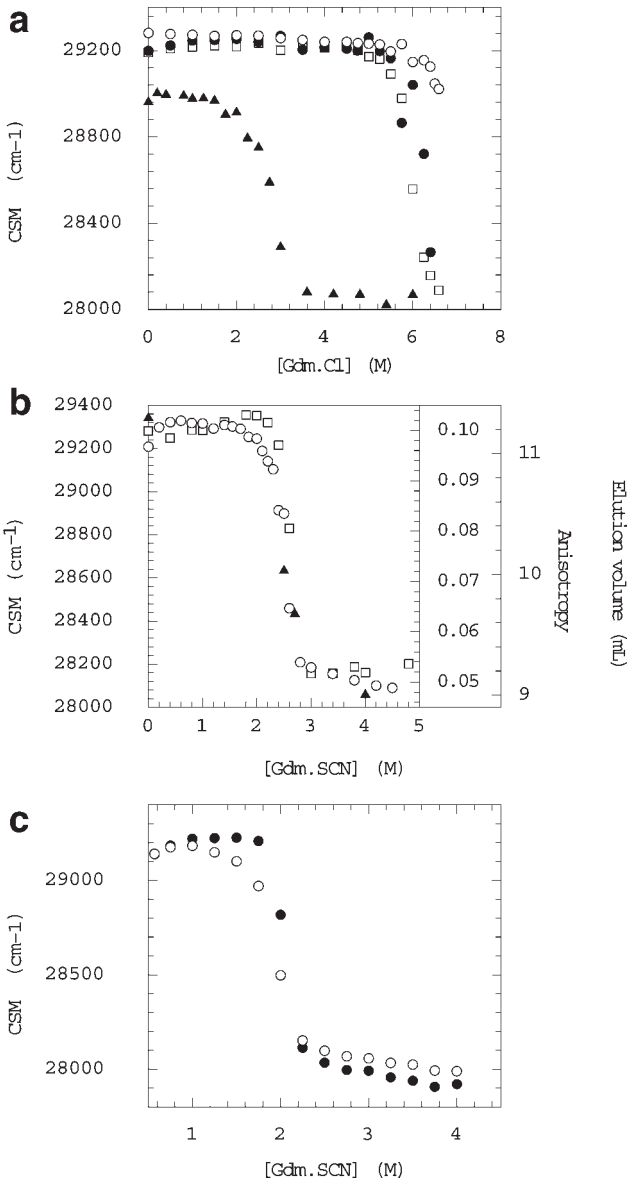

Figure 3
*Chemical denaturation of EBNA1$_{452–641}$. (**a**) Stability of EBNA1$_{452–641}$ to Gdm.Cl denaturation. In all cases the CSM was calculated from fluorescence emission between 300 and 450 nm. Three different pH 3 (black circle), 7 (white circle), and 10 (white square) were used for Gdm.Cl denaturation; stability of E2 at pH 7 is also shown (black triangle). [EBNA1$_{452–641}$] = [E2] = 0.5 μM. Buffers: 25 mM citrate/phosphate pH 3, and 0.2M NaCl, 25 mM bis-Tris HCl pH 7, and 0.2M NaCl and 25 mM NaHCO3/Na$_2$CO$_3$, and 0.2M NaCl. (**b**) Stability of EBNA1$_{452–641}$ to Gdm.SCN denaturation. CSM of EBNA1$_{452–641}$ was calculated from fluorescence emission between 300 and 450 nm at 2 h incubation (white circle). Trp Anisotropy was measured at 2 h incubation (white square). Protein concentration 2.5 μM; buffer, 25 mM bis-Tris HCl pH 7.0, with 0.2M NaCl and 1 mM DTT. The elution volume (mL) of EBNA1$_{452–641}$ was measured using a Superdex 75 column equilibrated at 0, 2.5, 2.7, and 4M Gdm.SCN concentrations (black triangle). Injection: 200 μL of 30 μM protein solution preincubated at the indicated denaturant concentrations. (**c**) Gradual refolding of unfolded EBNA1$_{452–641}$ at two different times, 2 h (white circle) and 24 h (black circle). [EBNA1$_{452–641}$]$_{initial}$ = 20 μM, [EBNA1$_{452–641}$]$_{refolded}$ = 2.9 μM, buffer, 25 mM bis-Tris HCl pH 7.0, with 0.2M NaCl and 1 mM DTT.*

DOI 10.1002/prot

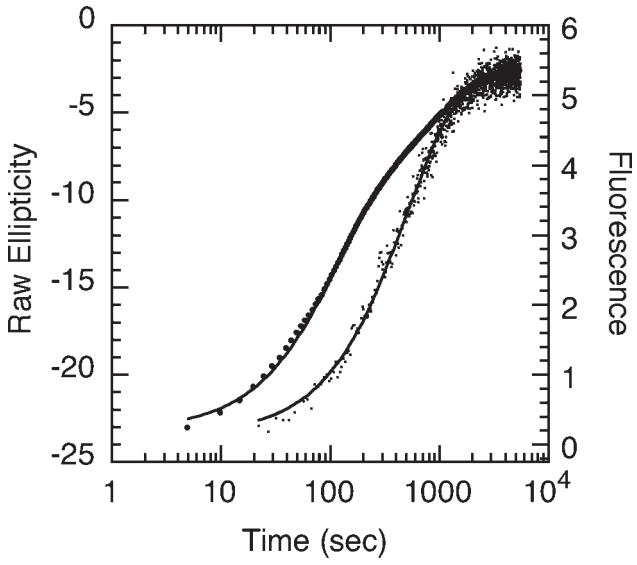

Figure 4

Unfolding Kinetics of EBNA1$_{452–641}$. Unfolding of EBNA1$_{452–641}$ followed by fluorescence emission at 335 nm (black circle) and raw ellipticity at 225 nm (dots). [EBNA1$_{452–641}$] = 4 μM, buffer 25 mM bis-Tris HCl pH 7, and 0.2M NaCl.

the end of the transition (4.0*M* Gdm.SCN) the domain is monomeric, as the molecular weight determined from static light scattering unequivocally indicates (Table I). To further investigate the unfolding transition, we determined the reversibility of the process by diluting Gdm.SCN unfolded EBNA1$_{452–641}$ gradually into different concentrations of the denaturant. Figure 3(c) shows that the unfolded EBNA1$_{452–641}$ domain recovers its folded CSM through an apparent identical route to the equilibrium unfolding process, suggesting an apparent reversibility in terms of fluorescence properties and solubility.

The slow unfolding was directly investigated following the time dependent changes after mixing the folded EBNA1$_{452–641}$ domain with Gdm.SCN. Both fluorescence and circular dichroism were monitored and the data are shown in Figure 4. A clear uncoupling of both probes is evident, most of the fluorescence change takes place before the ellipticity change, indicating that a loss in tertiary structure precedes the global unfolding of the secondary structure. The fluorescence change fits to at least two main exponential events accounting for 90% of the amplitude, with rates of 0.010 ± 0.0004 and 0.0012 ± 0.0006 s^{-1}, and a much slower event not dissectable at this stage. The ellipticity change involves one phase with rates of 0.0019 ± 0.0004 s^{-1}, in good agreement with one of the fluorescence phases. Thus, there appears to be a fast event with $t_{1/2} \sim 69$ s^{-1} involving only changes in tryptophan fluorescence, another event involving both tertiary and secondary structure changes with a $t_{1/2} \sim 9$ min from fluorescence and 6 min according to ellipticity change.

Unfolded EBNA1$_{452-641}$ refolds to soluble large spherical oligomers

Despite the full CSM recovery, the fluorescence spectrum of EBNA1$_{452–641}$ domain does not fully recover its folded intensity [Fig. 5(a)]. This can represent only a small change in a chromophore's environment, but we investigated the reversibility using CD. Upon dilution and dialysis of the protein unfolded in 4.0*M* Gdm.SCN, the far-UV CD spectrum corresponds to a folded species but it is different from the starting folded domain [Fig. 5(b)]. The similarity in the aspect of the spectrum, despite the substantial overall change in ellipticity, made us consider an oligomerization process. The refolded EBNA1$_{452–641}$ domain runs in the exclusion volume of a Superdex 75 (Pharmacia Biotech) gel filtration column [Fig. 5(c)]. The soluble oligomeric species was found to elute in the exclusion volume of various columns and was included in a Sephacryl 500 (Pharmacia Biotech), which allowed us to carry out a light scattering experiment. The light scattering data provide an average molecular weight of 1.23 ± 0.09 MDa and an average radius of 19 ± 2 nM (Table I). The plot of the radius versus elution time indicates a fairly monodisperse, thus homogeneous, size distribution.

Upon dilution of Gdm.SCN unfolded EBNA1$_{452–641}$ into folding conditions, there is a slow fluorescence change accompanying the refolding reaction [Fig. 5(d)]. Using exponential analysis as an approximation, the process contains at least two phases: one accounting for 65% of the fluorescent change with a rate of 0.003 s^{-1} and the other with a rate of 0.0004 s^{-1}. Because of the formation of the oligomers, the detailed dissection of the reaction is complex and not within the reach of the present work. For similar reasons, since the protein does not return to the dimeric folded state and because of the irreversibility of the reaction, we cannot use standard equilibrium analysis for the unfolding transition and obtain free energies of unfolding as a measure of the stability.

All calculations from light scattering assume a spherical shape of the oligomer; therefore, we wanted to confirm or discard assumptions on the molecular shape, and we made use of AFM. The untreated recombinant folded EBNA1$_{452–641}$ dimer appears as regular bodies of spherical shape, with a diameter of 13 nm [Fig. 6(a)], compared to 7 nm obtained from light scattering (Table I). This discrepancy is expected since the small size of the molecule under study approaches the size of the tip of the microscope, which "deforms" the aspect of the molecule, extending it.[34] The EBNA1$_{452–641}$ oligomers appear as spherical with a 45 nm diameter in excellent agreement with the 40 ± 4 nm obtained from light scattering

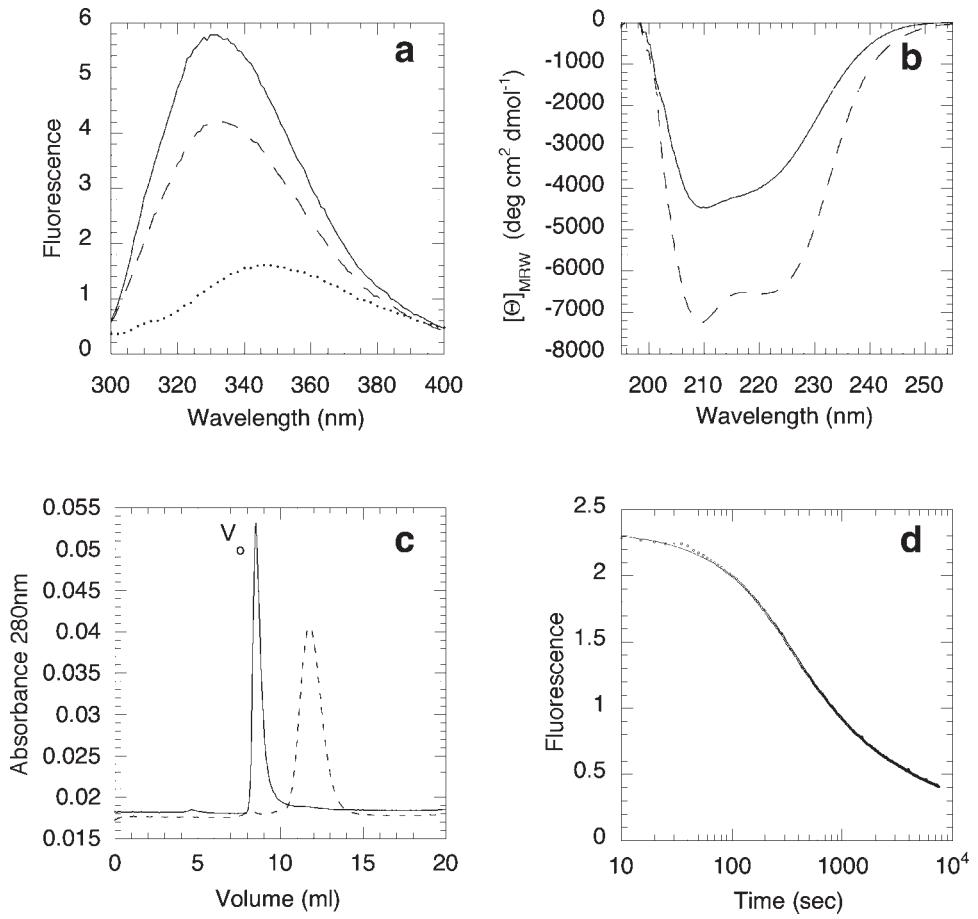

Figure 5

*Unfolded EBNA1$_{452–641}$ fully refolds into large soluble oligomers. (**a**) Reversibility of EBNA1$_{452–641}$ unfolding. EBNA1$_{452–641}$ was fully denatured in 4M Gdm.SCN and then diluted to lower the Gdm.SCN concentration to 0.4M to allow renaturation. CSM: 29,340 cm^{-1} for the native protein (continuous line), 28,193 cm^{-1} for the unfolded protein (dotted line), and 29,228 cm^{-1} for the refolded protein (dashed line). (**b**) CD spectra of EBNA1$_{452–641}$ (dimer, dashed line) and of the refolded species EBNA1$_{452–641}$-SOs (spherical oligomers, continuous line). [EBNA1$_{452–641}$] = 11 μM and [EBNA1$_{452–641}$-SOs] = 14 μM. Buffer: phosphate pH 7, 10 mM, 0.185M NaCl, and 1 mM DTT. (**c**) Gel filtration chromatography in a Superdex 75 Column of EBNA1$_{452–641}$ (dashed line) and of the refolded species EBNA1$_{452–641}$-SOs (continuous line). [EBNA1$_{452–641}$] = 14 μM and [EBNA1$_{452–641}$-SOs] = 14 μM. Buffer: 25 mM bis-Tris pH 7, 0.2M NaCl, and 1 mM DTT. (**d**) Refolding kinetics of EBNA1$_{452–641}$ in buffer 25 mM bis-Tris pH 7, 0.2M NaCl, and 1 mM DTT.*

[Fig. 6(b), Table I]. Figure 6(c) shows a three-dimensional image showing the regular shape of the EBNA1$_{452–641}$ spherical oligomers (EBNA1$_{452–641}$-SOs). In agreement with light scattering results, the size and shape of the oligomers appear highly homogeneous in all fields inspected.

Stability, amyloid like properties, and DNA binding of EBNA1$_{452-641}$-SOs

Anisotropy titration experiments show that EBNA1$_{452–641}$-SOs do not bind the EBNA site DNA in the concentration range that the dimeric domain does [Fig. 7(a)]. In addition, while the dimeric domain binds strongly to heparin affinity columns (see materials and methods), the oligomers do not bind at all (not shown).

The EBNA1$_{452–641}$-SOs were tested for their stability and were found, unlike the dimeric domain, to readily unfold cooperatively at low concentrations of Gdm.Cl, with an apparent $[D]_{50\%}$ of 3.0*M* against 6.8*M* for the dimer [Fig. 7(b)]. For a dimer that is so stable to thermal or chemical denaturation, it is quite intriguing that the Gdm.SCN unfolded protein fully refolds into an oligomeric form that is substantially less stable. We considered that the DNA could direct the folding route to the dimeric form if present at early stages of refolding. However, concentrations of EBNA1-DNA recognition site up to 10-fold in excess of the protein, still yield EBNA1$_{452–641}$-SOs, as judged by gel filtration and AFM (not shown).

The presence of large oligomers with decreased α-helical content made us investigate the possibility of repetitive β-sheet structure, as found in other spherical

DOI 10.1002/prot

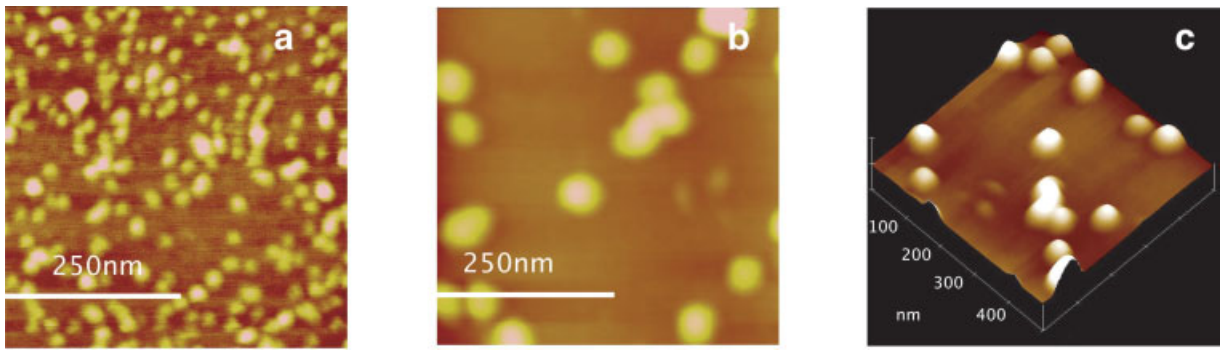

Figure 6

*AFM of EBNA1$_{452–641}$-SOs. (**a, b**) EBNA1$_{452–641}$ dimer and EBNA1$_{452–641}$-SOs absorbed onto a freshly cleaved mica under 10 mM buffer Hepes pH 7.5, and 1 mM $MgCl_2$. Top view (x, y: 500 nm; y: 1 and 10 nm). (**c**) EBNA1$_{452–641}$-SOs oligomer absorbed onto a freshly cleaved mica under 10 mM buffer Hepes pH 7.5, and 1 mM $MgCl_2$. Surface plot.*

oligomers.[35–37] For this purpose, we used Congo red and thioflavin-T, the reference dyes for repetitive β-sheet structure found in amyloids. EBNA1$_{452–641}$-SOs bind Congo red as the 20 nm shift in the spectrum indicates [Fig. 8(a)], and also produce a large fluorescence increase in thioflavin T, indicative of binding of this fluorophore [Fig. 8(b)].

DISCUSSION

Folding topology and function need not be related as the number of folds determined to date is very small when compared to the large number of biochemical functions found in natural proteins. In the case of the EBNA1 and HPV E2 DNA binding domains, they both recognize specific DNA sites in their respective genomes and perform similar functions in DNA replication, DNA segregation, and transcription regulation. However, their amino acid sequences are completely unrelated and so are the base sequences they recognize. Thus, a conservation of function is partial, but they share a unique dimeric β-barrel fold, suggesting that there must be other structural, possibly regulatory, events necessary for their function, beyond the recognition of DNA at their DNA binding sites. These events must, therefore, be related to folding, stability, and/or protein–protein interactions. With this in mind, we have been investigating both DNA binding and folding mechanism of HPV E2C[4–6,8,22,38,39] and EBNA1.[12]

The unfolding of dimeric proteins, in particular those with intertwined topologies such as the dimeric β-barrel,

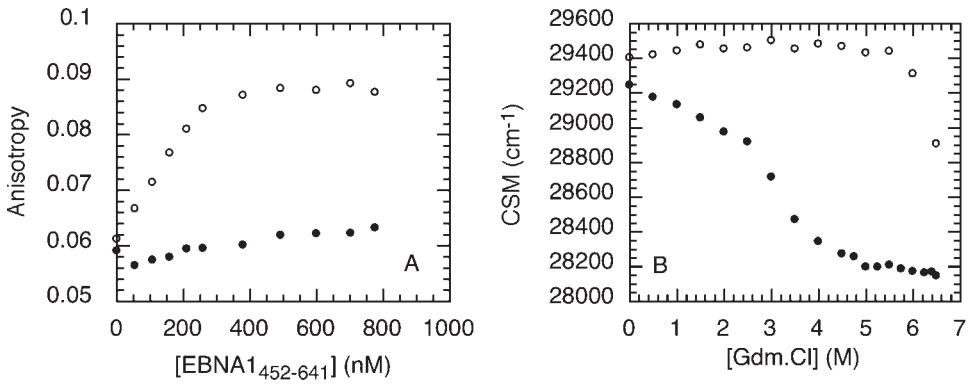

Figure 7

*Stability and DNA binding properties of EBNA1$_{452–641}$-SOs. (**a**) Binding experiment performed by adding EBNA1$_{452–641}$-SOs to a fixed amount of labeled oligonucleotide Site 1 5-FAM (black circle). Binding of EBNA1$_{452–641}$ dimer to the same oligonucleotide (white circle). (**b**) Stability of EBNA1$_{452–641}$-SOs oligomer to Gdm.Cl denaturation (black circle). Stability of EBNA1$_{452–641}$ dimer to Gdm.Cl denaturation (white circle). CSM was calculated from fluorescence emission between 300 and 450 nm.*

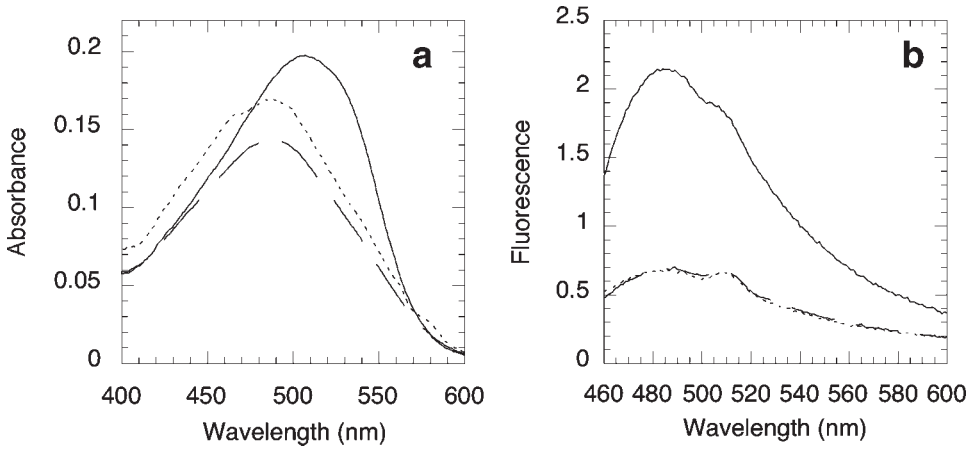

Figure 8

*Congo red and thioflavin binding by EBNA1$_{452–641}$-SOs. (**a**) Absorbance spectra of buffer (dashed line), EBNA1$_{452–641}$ (dotted line), and EBNA1$_{452–641}$-SOs (continuous line) with 5 μM Congo red. (**b**) Fluorescence spectra of blank (buffer plus thioflavin T) (dashed line), EBNA1$_{452–641}$ (dotted line), and EBNA1$_{452–641}$-SOs (continuous line) with 5 μM thioflavin T.*

is expected to depend on protein concentration given the dissociation added to the unfolding equilibria. Although this is the case for HPV16 E2C,[4,22] the EBNA1$_{452–641}$ domain does not show such dependence in the range allowed by a highly sensitive probe such as fluorescence ($\geq$0.1 μ*M* EBNA1$_{452–641}$). This suggests that the sum of the interactions that hold the barrel interface are at least as stable, and thus not dissectable, from those that hold the global fold. The slow uncoupling of tertiary and secondary structure upon unfolding together with the lack of protein concentration dependence suggest that the uncoupling of tertiary and secondary structure does not involve dissociation, or in other words, dissociation takes place together with global unfolding of secondary structure. The kinetic unfolding results suggest the presence of a dimeric intermediate where its tryptophan residues are accessible to the solvent, typical of loss of compact tertiary structure. The slow nature of the process and the strong uncoupling suggest that a characterization of such intermediate is amenable using various spectroscopic, even NMR, methods.

In fact, the fold is so stable that the SCN^- salt of guanidine (the stronger chemical denaturant accessible to standard laboratory use) is required to unfold it. Most secondary structure is retained even at temperatures as high as 90°C and pH below 3.0. At pH 3.0, the domain is still a dimer; we found no conditions where a monomer could be isolated or even detected, other than at high Gdm.SCN concentrations. However, the irreversibility in terms of the molecularity of the species and the lack of information of the stoichiometry of the oligomers precludes the analysis of the folding reaction in energetic terms. It is interesting to note that the EBNA1 protein is also extremely stable in cells, with no measurable turnover after 32 h.[40] While the lack of EBNA1 turnover is due at least in part to the central Gly-Ala repeat,[41] it is possible that the high stability of the DNA binding domain also interferes with EBNA1 processes by the proteasome. On the other hand, the less stable DNA binding domain of E2 does not appear to interfere with proteasomal processing, since E2 is much more labile with a half life of ~50 min.[42]

The unfolding reaction yields a fully soluble species, no aggregation is observed, and the CSM of the fluorescence spectra is fully reversible and through the same apparent route in equilibrium refolding experiments. However, the monomeric unfolded domain returns in full to large spherical oligomers, thus the reaction is not actually reversible since it does not return to the dimeric native state. We were not able to obtain folded dimers under different pH and protein concentrations, including the addition of excess of specific DNA presence with the intention to "guide" the folding. The refolding kinetics is relatively multiexponential and involves oligomerization, requiring a more detailed analysis due to its complexity.

Light scattering provided a value of ~1.2 MDa for the oligomers and a simple estimation based on the molecular weight of the EBNA1$_{452–641}$ polypeptide only indicates ~57 monomers per mole of oligomer. However, a deeper characterization would be required considering the compactness of the oligomers and conformation of the monomers. The sizes of the EBNA1$_{452–641}$-SOs from light scattering and AFM coincide in ~40–45 nm spheres. The slow nature of the process and the possibility of further slowing it down by solvent manipulation or temperature may allow to determine how and when the actual oligomerization takes place. The EBNA1$_{452–641}$-SOs do not bind DNA, and they are not capable of binding to

DOI 10.1002/prot

immobilized heparin, unlike the folded dimer (not shown). This, together with the substantial reduction in the negative α-helical signal in the far-UV CD, suggests that the secondary structure of the oligomers is different from that of the dimers. There appears to be early events that cause the unfolded monomers to arrange into oligomers instead of the hyperstable dimers. These results strongly suggest that the oligomers are assembled from modified monomers rather than oligomerized dimers. The coincident CSM suggest that the level of burial of the trp residues is similar and some regions may retain substantial native conformation. The ability of the oligomers to bind Congo red and thioflavin T indicates the presence of repetitive β-sheet structure similar to that found in amyloid fibers and their oligomeric soluble precursors, something not found in the dimers. Several proteins of different nature were described to self-assemble into spherical oligomers,[43–45] and this property can also take place in natively unfolded proteins.[35,46] In the case of the $EBNA1_{452–641}$ domain, there is no evident implication in an amyloid route, and likely represents a kinetically stable species, which shares properties with amyloid oligomeric intermediates. In any case we have not attempted to force an insoluble amyloid route, something that may potentially be attained.

In most cases, these structures emerge from existing equilibria of folded states of proteins, where local unfolding or marginally stable structures slowly self-assemble into β-sheet oligomers that finally lead to the irreversible formation of insoluble fibers.[47] We have recently described an amyloid route upon a very small solvent perturbation in the HPV16 E2 DNA binding domain, which leads to the formation of curly-like fibers, through the formation of soluble intermediates with a large increase in β-sheet content.[48] The E2 DNA binding domain is much less stable than the $EBNA1_{452–641}$ domain and this could be the basis for which the latter can form the oligomeric species only after substantial unfolding required for dissociation to monomers. We previously determined that a partly folded monomer of E2c could be possible.[7]

By comparing $[Gdm.SCN]_{50\%}$ we can conclude that the $EBNA1_{452–641}$-SOs are much less stable than the dimers but show cooperativity, which indicates compactness, supported by the full recovery of the CSM, indicative of tryptophan burial. However, no increase in β-sheet content is observed from the CD spectra. An interesting aspect of the $EBNA1_{452–641}$-SOs is that they are stable and do not progress into amyloid fibers in the conditions used so far. The EBNA1 SOs are therefore more amenable to characterization, in contrast to the prefibrilar oligomers found in most amyloid routes, which are difficult to study because of their transient nature. Based on the substantial secondary structure change, the lack of DNA binding capacity, and the lower stability of the $EBNA1_{452–641}$-SOs, we conclude that there is a large conformational rearrangement in $EBNA1_{452–641}$-SOs, which must result in a rather different topology.

Irrespective of the biological implications, the recombinant protein is synthesized in bacteria and readily acquires its hyperstable dimeric β-barrel structure. However, the refolding from the unfolded polypeptide does not yield the most thermodynamically stable species, but completely assembles into oligomeric, albeit less stable, species. This means that with the full sequence information, and in the absence of putative folding accessory proteins found in the bacterial cytosol, the protein does not yield the dimeric highly stable form. Alternatively, there could be co-translational N- to C-terminus directed partial folding events that ensure the most stable dimeric conformation. The folding kinetics is not fast, in fact it is rather slow ($t_{1/2} \sim 30$ min), but still drives the molecules into the oligomerization route, despite efforts at different pHs, protein concentration, or the addition of specific DNA to stabilize the early native conformation of the DNA binding site.

Our results suggest that the folding of EBNA1 into the dimeric form is assisted by proteins acting co-translationally, or could occur directionally from N- to C-terminus. However, it is possible that under certain circumstances, such as high levels of viral gene expression, the folding assisting machinery may not be able to cope with the increased levels of polypeptides being synthesized. Such a situation could occur in EBV lytic infection. Unlike the other EBV latency proteins, EBNA1 continues to be expressed in lytic infection, although its role on origin binding is no longer required. It is possible that the EBNA1 produced at this time may be in the spherical oligomer form, which may fulfill a distinct function particular to lytic infection.

The extreme stability of this domain addresses fundamental issues of protein folding as to why the much less stable oligomeric species are the product of the refolding, clearly a kinetic as opposed to thermodynamically driven reaction. An additional issue to be addressed is why the $EBNA1_{452–641}$ is so much more stable than the HPV E2 dimeric β-barrel. Interestingly, the "kinetically trapped" oligomers share properties with prefibrilar amyloid intermediates and have the advantage of being stable, which provide the prospect of a detailed characterization. The recent report of a functional amyloid formation supports the hypothesis that "amyloid" is an evolved quaternary protein fold used by organisms from bacteria to humans not exclusive of misfolding diseases or pathological situations.[49] Finally, the possible presence of the $EBNA1_{452–641}$-SOs in infected cells and their connection with the progress of disease remains to be established through the development of selective tools such as monoclonal antibodies capable of discriminating conformers.

ACKNOWLEDGMENTS

GPG is a Career Investigator from CONICET.

REFERENCES

1. Bochkarev A, Barwell JA, Pfuetzner RA, Furey W, Jr, Edwards AM, Frappier L. Crystal structure of the DNA-binding domain of the Epstein-Barr virus origin-binding protein EBNA 1. Cell 1995;83:39–46.
2. Bochkarev A, Barwell JA, Pfuetzner RA, Bochkareva E, Frappier L, Edwards AM. Crystal structure of the DNA-binding domain of the Epstein-Barr virus origin-binding protein. EBNA1, bound to DNA Cell 1996;84:791–800.
3. Hegde RS, Grossman SR, Laimins LA, Sigler PB. Crystal structure at 1.7 A of the bovine papillomavirus-1 E2 DNA-binding domain bound to its DNA target. Nature 1992;359:505–512.
4. Mok YK, de Prat-Gay G, Butler PJ, Bycroft M. Equilibrium dissociation and unfolding of the dimeric human papillomavirus strain-16 E2 DNA-binding domain. Protein Sci 1996;5:310–319.
5. Mok YK, Bycroft M, de Prat-Gay G. The dimeric DNA binding domain of the human papillomavirus E2 protein folds through a monomeric intermediate which cannot be native-like. Nat Struct Biol 1996;3:711–717.
6. Lima LM, Prat-Gay G. Conformational changes and stabilization induced by ligand binding in the DNA-binding domain of the E2 protein from human papillomavirus. J Biol Chem 1997;272:19295–19303.
7. Foguel D, Silva JL, de Prat-Gay G. Characterization of a partially folded monomer of the DNA-binding domain of human papillomavirus E2 protein obtained at high pressure. J Biol Chem 1998;273:9050–9057.
8. Mok YK, Alonso LG, Lima LM, Bycroft M, de Prat-Gay G. Folding of a dimeric beta-barrel: residual structure in the urea denatured state of the human papillomavirus E2 DNA binding domain. Protein Sci 2000;9:799–811.
9. Barwell JA, Bochkarev A, Pfuetzner RA, Tong H, Yang DS, Frappier L, Edwards AM. Overexpression, purification, and crystallization of the DNA binding and dimerization domains of the Epstein-Barr virus nuclear antigen 1. J Biol Chem 1995;270:20556–20559.
10. Ceccarelli DF, Frappier L. Functional analyses of the EBNA1 origin DNA binding protein of Epstein-Barr virus. J Virol 2000;74:4939–4948.
11. Summers H, Barwell JA, Pfuetzner RA, Edwards AM, Frappier L. Cooperative assembly of EBNA1 on the Epstein-Barr virus latent origin of replication. J Virol 1996;70:1228–1231.
12. Oddo C, Freire E, Frappier L, de Prat-Gay G. Mechanism of DNA recognition at a viral replication origin. J Biol Chem 2006;281:26893–26903.
13. Plaxco KW, Simons KT, Ruczinski I, Baker D. Topology, stability, sequence, and length: defining the determinants of two-state protein folding kinetics. Biochemistry 2000;39:11177–11183.
14. Daggett V, Fersht A. The present view of the mechanism of protein folding. Nat Rev Mol Cell Biol 2003;4:497–502.
15. Jaenicke R. Stability and folding of domain proteins. Prog Biophys Mol Biol 1999;71:155–241.
16. Jaenicke R, Lilie H. Folding and association of oligomeric and multimeric proteins. Adv Protein Chem 2000;53:329–401.
17. Banks DD, Gloss LM. Folding mechanism of the (H3-H4)2 histone tetramer of the core nucleosome. Protein Sci 2004;13:1304–1316.
18. Milla ME, Sauer RT. P22 Arc repressor: folding kinetics of a single-domain, dimeric protein. Biochemistry 1994;33:1125–1133.
19. Srivastava AK, Sauer RT. Evidence for partial secondary structure formation in the transition state for arc repressor refolding and dimerization. Biochemistry 2000;39:8308–8314.
20. Zitzewitz JA, Bilsel O, Luo J, Jones BE, Matthews CR. Probing the folding mechanism of a leucine zipper peptide by stopped-flow circular dichroism spectroscopy. Biochemistry 1995;34:12812–12819.
21. Zitzewitz JA, Ibarra-Molero B, Fishel DR, Terry KL, Matthews CR. Preformed secondary structure drives the association reaction of GCN4-p1, a model coiled-coil system. J Mol Biol 2000;296:1105–1116.
22. Prat-Gay G, Nadra AD, Corrales-Izquierdo FJ, Alonso LG, Ferreiro DU, Mok YK. The folding mechanism of a dimeric beta-barrel domain. J Mol Biol 2005;351:672–682.
23. Kim PS, Baldwin RL. Intermediates in the folding reactions of small proteins. Annu Rev Biochem 1990;59:631–660.
24. Kim DH, Jang DS, Nam GH, Choi KY. Folding mechanism of ketosteroid isomerase from Comamonas testosteroni. Biochemistry 2001;40:5011–5017.
25. Gittelman MS, Matthews CR. Folding and stability of trp aporepressor from Escherichia coli. Biochemistry 1990;29:7011–7020.
26. Mann CJ, Shao X, Matthews CR. Characterization of the slow folding reactions of trp aporepressor from Escherichia coli by mutational analysis of prolines and catalysis by a peptidyl-prolyl isomerase. Biochemistry 1995;34:14573–14580.
27. Gloss LM, Simler BR, Matthews CR. Rough energy landscapes in protein folding: dimeric E. coli Trp repressor folds through three parallel channels. J Mol Biol 2001;312:1121–1134.
28. Wallace LA, Sluis-Cremer N, Dirr HW. Equilibrium and kinetic unfolding properties of dimeric human glutathione transferase A1-1. Biochemistry 1998;37:5320–5328.
29. Wallace LA, Dirr HW. Folding and assembly of dimeric human glutathione transferase A1-1. Biochemistry 1999;38:16686–16694.
30. Clark AC, Raso SW, Sinclair JF, Ziegler MM, Chaffotte AF, Baldwin TO. Kinetic mechanism of luciferase subunit folding and assembly. Biochemistry 1997;36:1891–1899.
31. Noland BW, Dangott LJ, Baldwin TO. Folding, stability, and physical properties of the alpha subunit of bacterial luciferase. Biochemistry 1999;38:16136–16145.
32. Inlow JK, Baldwin TO. Mutational analysis of the subunit interface of Vibrio harveyi bacterial luciferase. Biochemistry 2002;41:3906–3915.
33. Weber G, Teale FWJ. Interactions of proteins with radiation. In: Weissbluth E, editor. The proteins, Vol III. New York: Academic Press; 2nd ed., 1965. pp 369–396.
34. Schneider SW, Larmer J, Henderson RM, Oberleithner H. Molecular weights of individual proteins correlate with molecular volumes measured by atomic force microscopy. Pflugers Arch 1998;435:362–367.
35. Chen YR, Glabe CG. Distinct early folding and aggregation properties of alzheimer amyloid-beta peptide Abeta 40 and Abeta 42: stable trimer or tetramer formation by Abeta 42. J Biol Chem 2006.
36. Alonso LG, Garcia-Alai MM, Smal C, Centeno JM, Iacono R, Castano E, Gualfetti P, de Prat-Gay G. The HPV16 E7 viral oncoprotein self-assembles into defined spherical oligomers. Biochemistry 2004;43:3310–3317.
37. Carrotta R, Bauer R, Waninge R, Rischel C. Conformational characterization of oligomeric intermediates and aggregates in β-lactoglobulin heat aggregation. Protein Sci 2001;10:1312–1318.
38. Ferreiro DU, Lima LM, Nadra AD, Alonso LG, Goldbaum FA, de Prat-Gay G. Distinctive cognate sequence discrimination, bound DNA conformation, and binding modes in the E2 C-terminal domains from prototype human and bovine papillomaviruses. Biochemistry 2000;39:14692–14701.
39. Ferreiro DU, de Prat-Gay G. A protein-DNA binding mechanism proceeds through multi-state or two-state parallel pathways. J Mol Biol 2003;331:89–99.
40. Holowaty MN, Zeghouf M, Wu H, Tellam J, Athanasopoulos V, Greenblatt J, Frappier L. Protein profiling with Epstein-Barr nuclear antigen-1 reveals an interaction with the herpesvirus-associated ubiquitin-specific protease HAUSP/USP7. J Biol Chem 2003;278:29987–29994.
41. Fahraeus R. Do peptides control their own birth and death? Nat Rev Mol Cell Biol 2005;6:263–267.
42. Penrose KJ, McBride AA. Proteasome-mediated degradation of the papillomavirus E2-TA protein is regulated by phosphorylation and can modulate viral genome copy number. J Virol 2000;74:6031–6038.

DOI 10.1002/prot

43. Kentsis A, Gordon RE, Borden KL. Self-assembly properties of a model RING domain. Proc Natl Acad Sci USA 2002;99:667–672.
44. Meyer SC, Huerta C, Ghosh I. Single-site mutations in a hyperthermophilic variant of the B1 domain of protein G result in self-assembled oligomers. Biochemistry 2005;44:2360–2368.
45. Vauthey S, Santoso S, Gong H, Watson N, Zhang S. Molecular self-assembly of surfactant-like peptides to form nanotubes and nanovesicles. Proc Natl Acad Sci USA 2002;99:5355–5360.
46. Fink AL. Natively unfolded proteins. Curr Opin Struct Biol 2005;15:35–41.
47. Dobson CM. Principles of protein folding, misfolding and aggregation. Semin Cell Dev Biol 2004;15:3–16.
48. Wetzler DE, Castaño EM, Prat Gay G. A quasi-spontaneous amyloid route in a DNA binding gene regulatory domain: the papillomavirus HPV 16 E2 protein. Protein Sci 2007;16:744–754.
49. Fowler DM, Koulov AV, Alory-Jost C, Marks MS, Balch WE, Kelly JW Functional amyloid formation within mammalian tissue. PLo S Biol 2006;4:e6.